nature portfolio

https://doi.org/10.1038/s41586-025-09053-4

Supplementary information

Cross-tissue multicellular coordination and its rewiring in cancer

In the format provided by the authors and unedited

Supplementary Information for

Cross-tissue multicellular coordination and its rewiring in cancer

Qiang Shi[1,4*], Yihan Chen[1,4], Yang Li[1], Shishang Qin[1], Yu Yang[1,2], Yang Gao[3], Linnan Zhu[1], Dongfang Wang[1] & Zemin Zhang[1,2*]

[1]Biomedical Pioneering Innovation Center (BIOPIC), School of Life Sciences, and Academy for Advanced Interdisciplinary Studies, Peking University, Beijing 100871, China

[2]Chongqing Medical University, Chongqing 400016, China

[3]Institute of Cancer Research, Shenzhen Bay Laboratory, Shenzhen 518132, China

[4]These authors contributed equally: Qiang Shi, Yihan Chen.

[*]E-mail: zemin@pku.edu.cn; shiq@pku.edu.cn

Table of Contents

Supplementary Figures **2**

Supplementary Fig. 1 | Data integration and cell annotations. 2
Supplementary Fig. 2 | Tissue prevalence of cell subsets. 4
Supplementary Fig. 3 | Diversity of fibroblasts and epithelial cells. 5
Supplementary Fig. 4 | Global correlation network. 6
Supplementary Fig. 5 | CM activities. 8
Supplementary Fig. 6 | Associations between CM activity and phenotypic factors. 9
Supplementary Fig. 7 | DIALOGUE analysis of CM12. 10
Supplementary Fig. 8 | Pan-cancer cell annotations. 12
Supplementary Fig. 9 | CM08 program and cytokine analysis. 13
Supplementary Fig. 10 | Clinical implications of CM08 program. 15

Supplementary Notes **16**

Supplementary Note 1 | Linking CM activity to phenotypes 16
Supplementary Note 2 | A healthy multicellular program linked to cancer immunotherapy 16

Supplementary Table legends **18**

Supplementary References **19**

Supplementary Figures

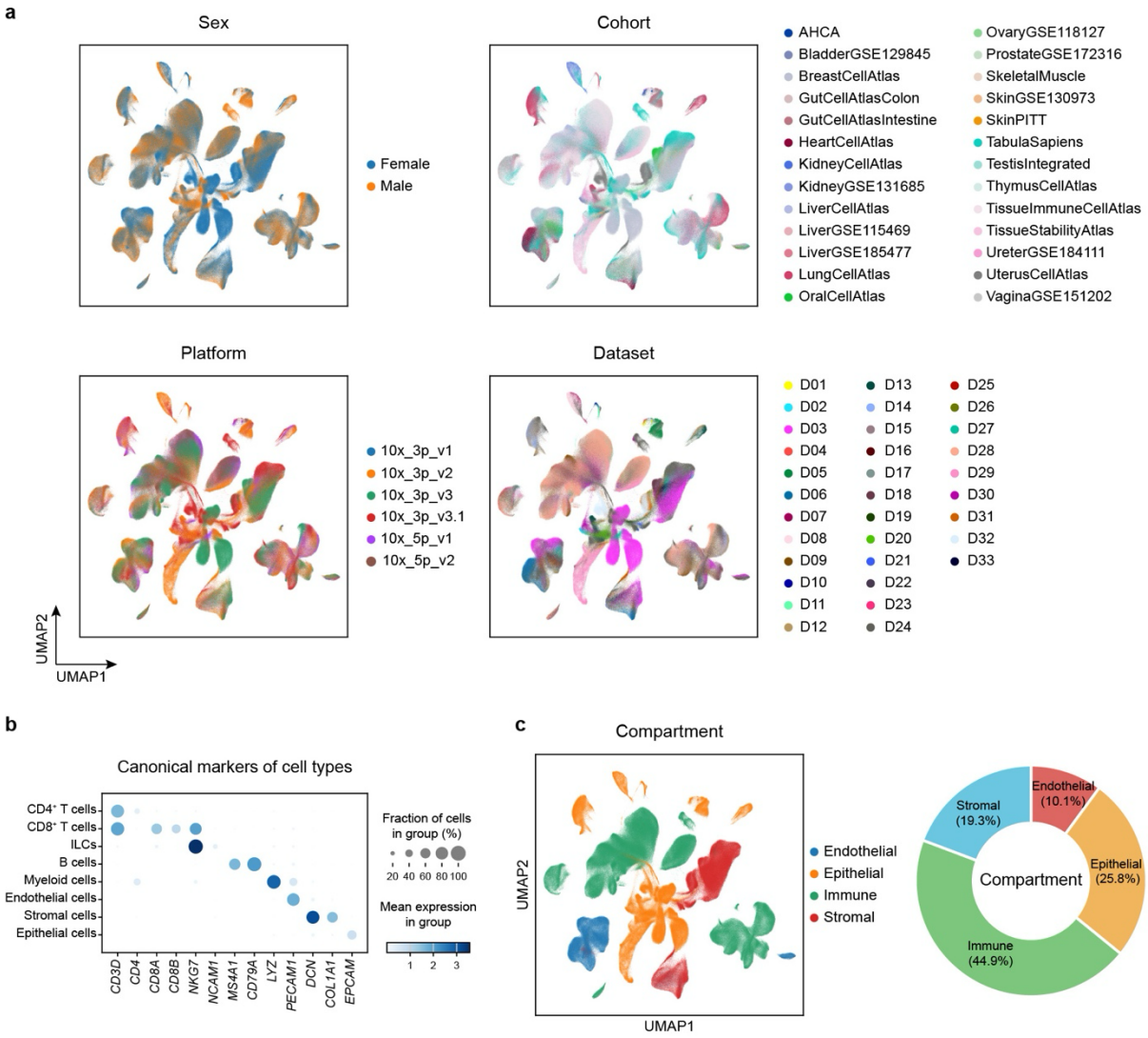

Supplementary Fig. 1 | Data integration and cell annotations.

(**a**) UMAP visualization of total cells colored by sex, platform, cohort, or dataset. (**b**) Dot plot showing the expression of canonical markers for cell types. (**c**) Cellular compartment annotations from the original studies, displayed as a UMAP visualization (left) and pie chart showing their percentages (right).

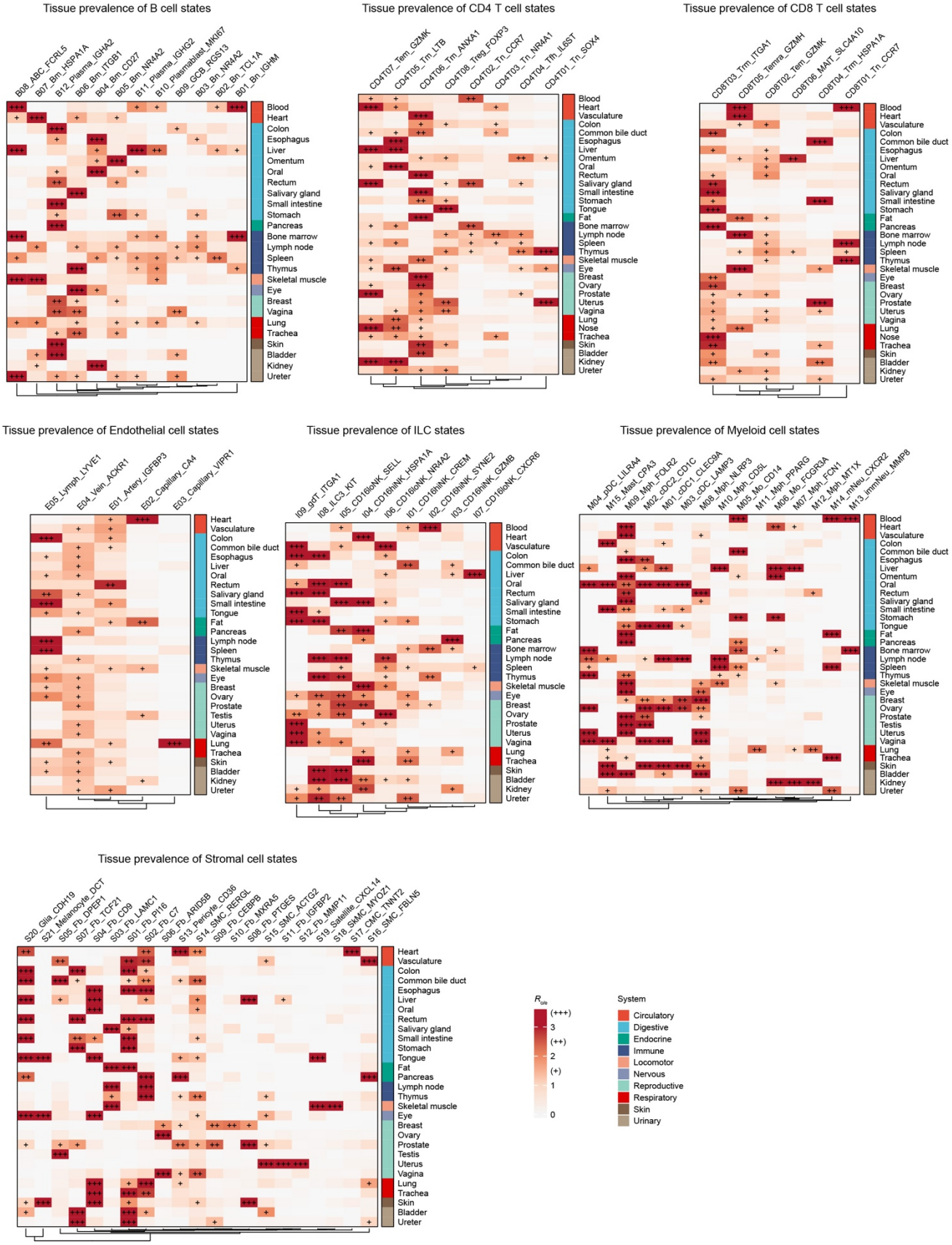
Tissue prevalence of B cell states
B08_ABC_FCRL5
B07_Bm_HSPA1A
B12_Plasma_IGHA2
B06_Bm_ITGB1
B04_Bm_CD27
B05_Bm_NR4A2
B11_Plasma_IGHG2
B10_Plasmablast_MKI67
B09_GCB_RGS13
B03_Bn_NR4A2
B02_Bn_TCL1A
B01_Bn_IGHM
Tissue prevalence of CD4 T cell states
CD4T07_Tem_GZMK
CD4T05_Tm_LTB
CD4T06_Tm_ANXA1
CD4T08_Treg_FOXP3
CD4T02_Tn_CCR7
CD4T03_Tn_NR4A1
CD4T04_Tfh_IL6ST
CD4T01_Tn_SOX4
Tissue prevalence of CD8 T cell states
CD8T03_Trm_ITGA1
CD8T05_Temra_GZMH
CD8T02_Tem_GZMK
CD8T06_MAIT_SLC4A10
CD8T04_Trm_HSPA1A
CD8T01_Tn_CCR7
Blood
Heart
Vasculature
Colon
Common bile duct
Esophagus
Liver
Omentum
Oral
Rectum
Salivary gland
Small intestine
Stomach
Tongue
Fat
Pancreas
Bone marrow
Lymph node
Spleen
Thymus
Skeletal muscle
Eye
Breast
Ovary
Prostate
Uterus
Vagina
Nose
Lung
Trachea
Skin
Bladder
Kidney
Ureter
Tissue prevalence of Endothelial cell states
E05_Lymph_LYVE1
E04_Vein_ACKR1
E01_Artery_IGFBP3
E02_Capillary_CA4
E03_Capillary_VIPR1
Tissue prevalence of ILC states
I09_gdT_ITGA1
I08_ILC3_KIT
I05_CD16loNK_SELL
I04_CD16hiNK_HSPA1A
I06_CD16loNK_NR4A2
I01_CD16hiNK_CREM
I02_CD16hiNK_SYNE2
I03_CD16hiNK_GZMB
I07_CD16loNK_CXCR6
Tissue prevalence of Myeloid cell states
M04_pDC_LILRA4
M15_Mast_CPA3
M09_Mph_FOLR2
M02_cDC2_CD1C
M01_cDC1_CLEC9A
M03_cDC_LAMP3
M08_Mph_NLRP3
M10_Mph_CD5L
M05_Mo_CD14
M11_Mph_PPARG
M06_Mo_FCGR3A
M07_Mph_FCN1
M12_Mph_MT1X
M14_mNeu_CXCR2
M13_immNeu_MMP8
Tissue prevalence of Stromal cell states
S20_Glia_CDH19
S21_Melanocyte_DCT
S05_Fb_DPEP1
S07_Fb_TCF21
S04_Fb_CD9
S03_Fb_LAMC1
S01_Fb_PI16
S02_Fb_C7
S06_Fb_ARIDB
S13_Pericyte_CD36
S14_SMC_RERGL
S09_Fb_CEBPB
S10_Fb_MXRA5
S08_Fb_PTGES
S15_SMC_ACTG2
S11_Fb_IGFBP2
S12_Fb_MMP11
S19_Satellite_CXCL14
S18_SMC_MYOZ1
S17_CMC_TNNT2
S16_SMC_FBLN5
R_{ore}
(+++)
3
(++)
2
(+)
1
0
System
Circulatory
Digestive
Endocrine
Immune
Locomotor
Nervous
Reproductive
Respiratory
Skin
Urinary

Supplementary Fig. 2 | Tissue prevalence of cell subsets.

Tissue prevalence of cell subsets measured by $R_{o/e}$ for each cell type. Tissues are categorized and ordered by body systems.

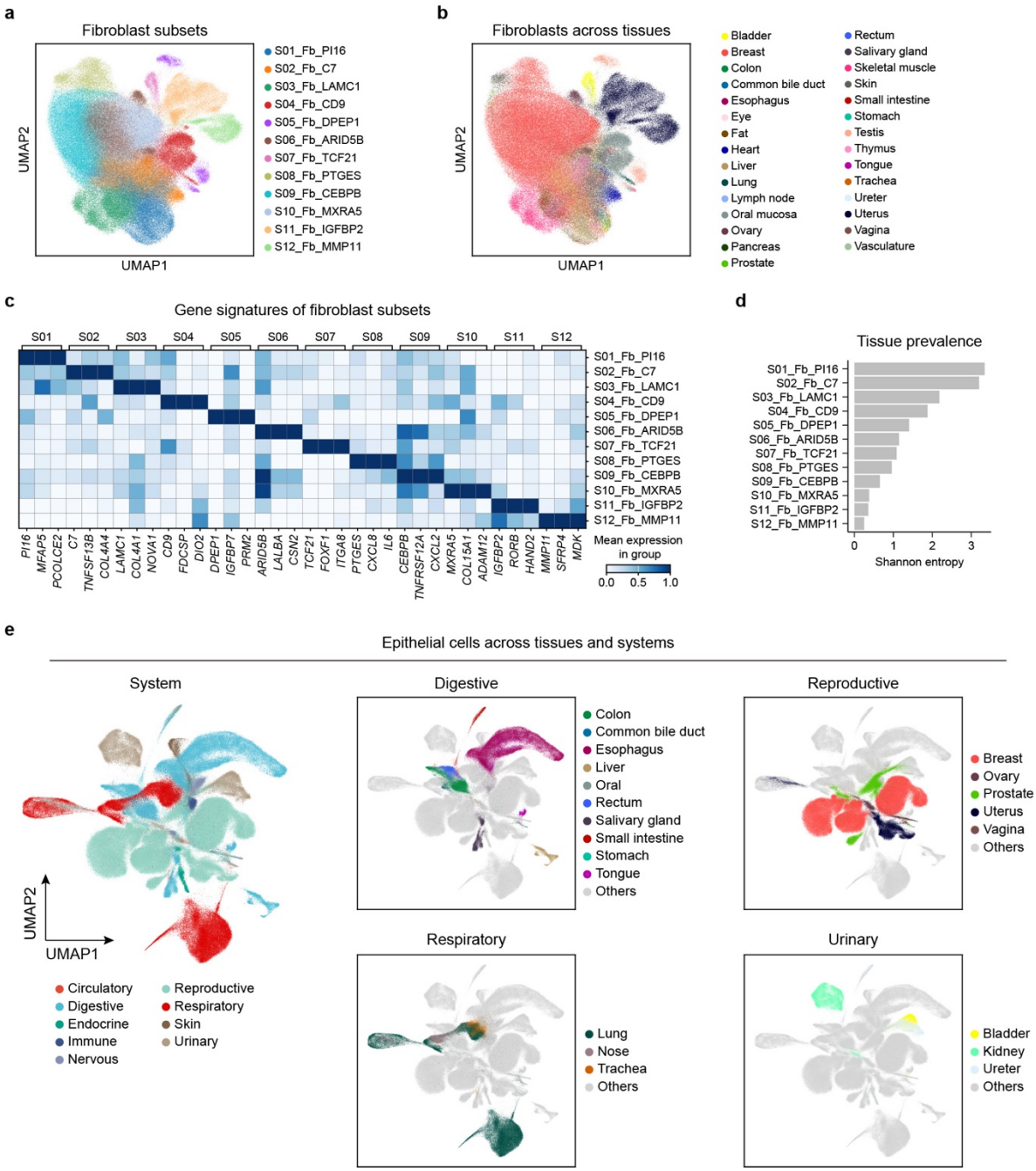

Supplementary Fig. 3 | Diversity of fibroblasts and epithelial cells.

(**a-b**) UMAP visualization of fibroblasts colored by subsets (**a**) or tissues (**b**). (**c**) Heatmap showing the scaled expression of selected signature genes in fibroblast subsets. (**d**) Bar plot showing the Shannon equitability of fibroblast subsets across tissues. (**e**) UMAP visualization of epithelial cells colored by body systems (left) or by tissues within individual systems (right).

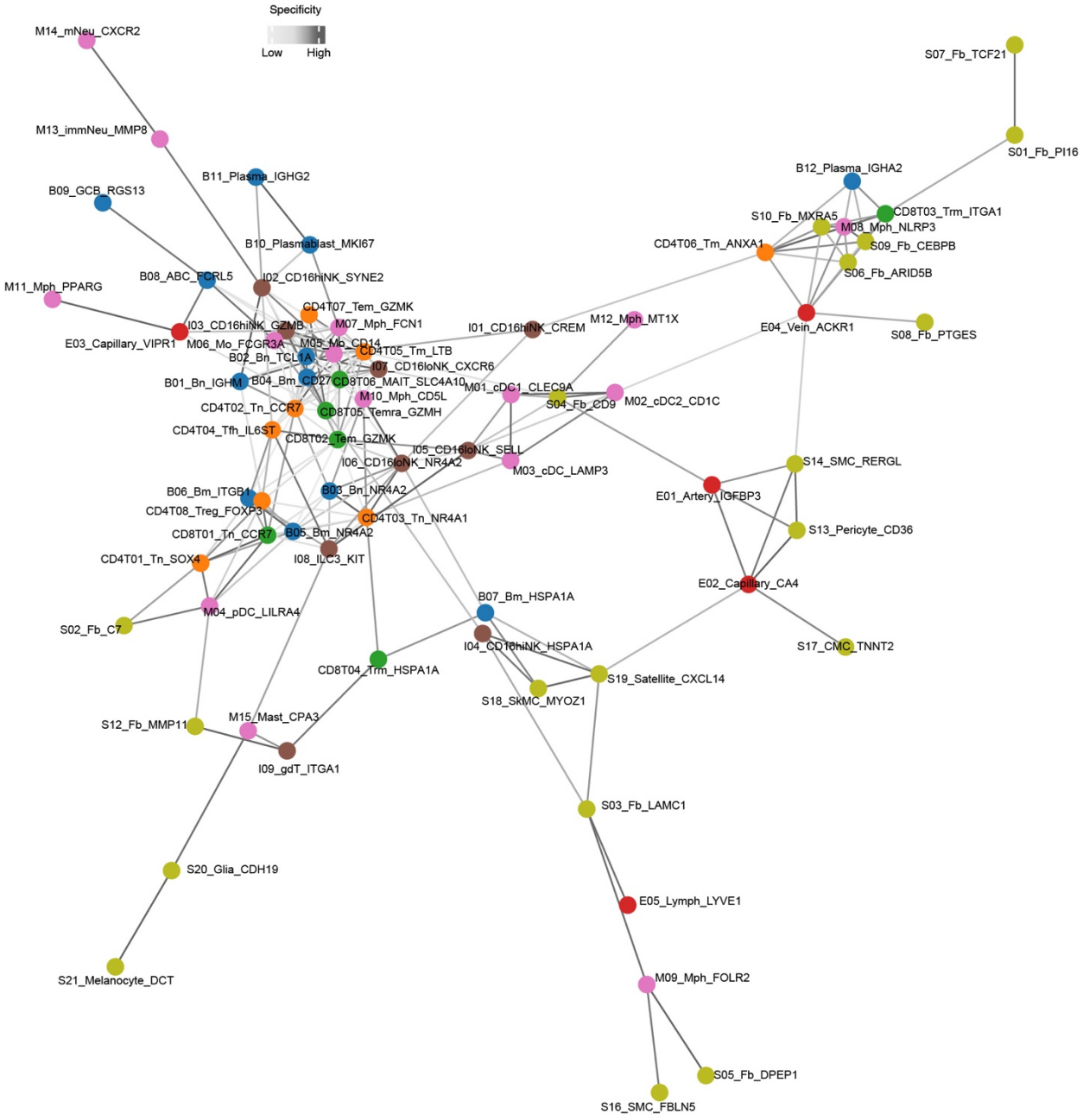

Supplementary Fig. 4 | Global correlation network.

Global network of specifically correlated subset pairs. Nodes represent cell subsets colored by cell types. Edge color indicates correlation specificity.

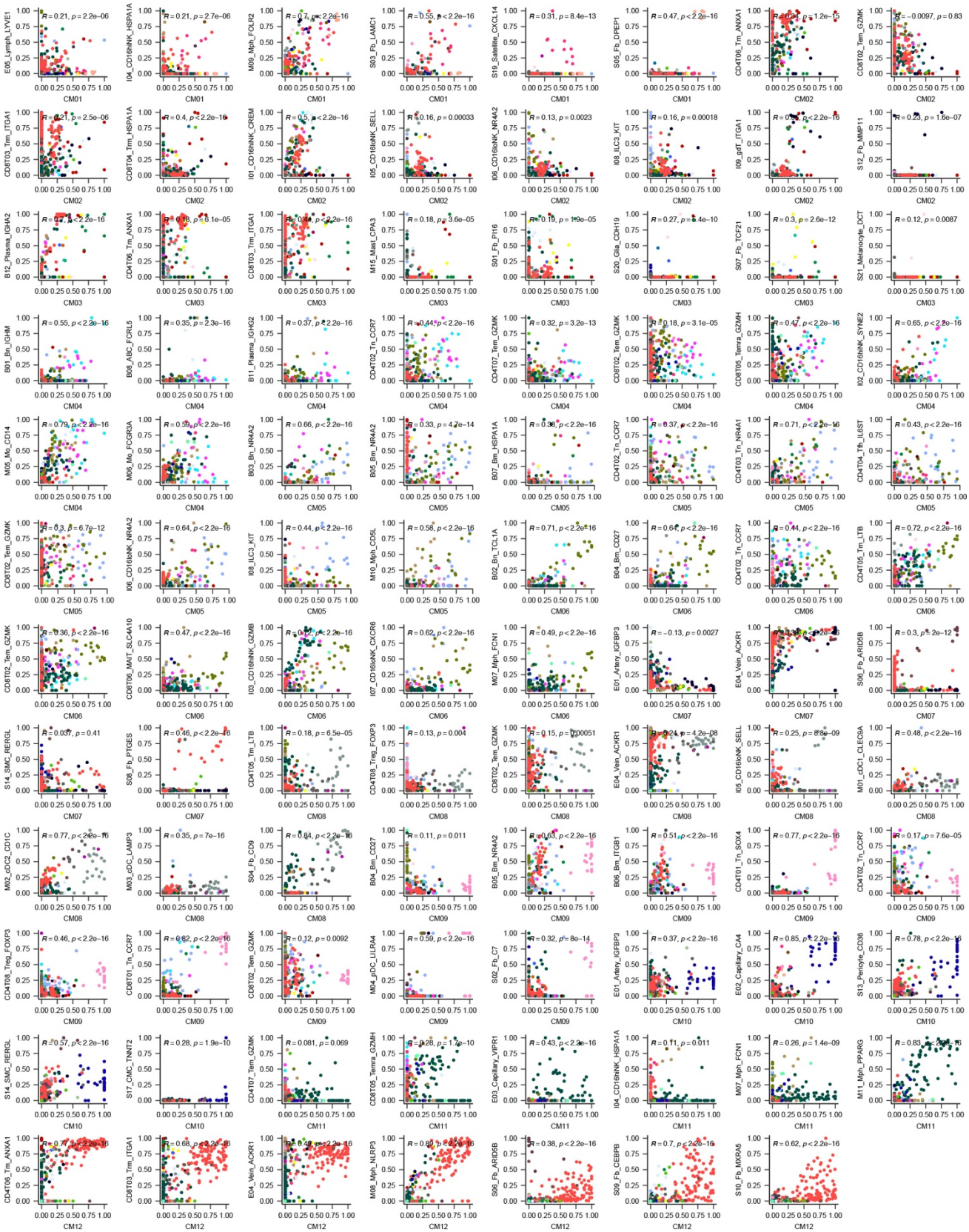
E05_Lymph_LYVE1
I04_CD16hiNK_HSPA1A
M09_Mph_FOLR2
S03_Fb_LAMC1
S19_Satellite_CXCL14
S05_Fb_DPEP1
CD4T06_Tm_ANXA1
CD8T02_Tem_GZMK
CD8T03_Tm_ITGA1
CD8T04_Tm_HSPA1A
I01_CD16hiNK_CREM
I05_CD16loNK_SELL
I06_CD16loNK_NR4A2
I08_ILC3_KIT
I09_gdT_ITGA1
S12_Fb_MMP11
B12_Plasma_IGHA2
CD4T06_Tm_ANXA1
CD8T03_Tm_ITGA1
M15_Mast_CPA3
S01_Fb_PI16
S20_Glia_CDH19
S07_Fb_TCF21
S21_Melanocyte_DCT
B01_Bn_IGHM
B08_ABC_FCRL5
B11_Plasma_IGHG2
CD4T02_Tn_CCR7
CD4T07_Tem_GZMK
CD8T02_Tem_GZMK
CD8T05_Temra_GZMH
I02_CD16hiNK_SYNE2
M05_Mo_CD14
M06_Mo_FCGR3A
B03_Bn_NR4A2
B05_Bm_NR4A2
B07_Bm_HSPA1A
CD4T02_Tn_CCR7
CD4T03_Tn_NR4A1
CD4T04_Th_IL6ST
CD8T02_Tem_GZMK
I06_CD16loNK_NR4A2
I08_ILC3_KIT
M10_Mph_CD5L
B02_Bn_TCL1A
B04_Bm_CD27
CD4T02_Tn_CCR7
CD4T05_Tm_LTB
CD8T02_Tem_GZMK
CD8T06_MAIT_SLC4A10
I03_CD16hiNK_GZMB
I07_CD16loNK_CXCR6
M07_Mph_FCN1
E01_Artery_IGFBP3
E04_Vein_ACKR1
S06_Fb_ARID5B
S14_SMC_RERGL
S08_Fb_PTGES
CD4T05_Tm_LTB
CD4T08_Treg_FOXP3
CD8T02_Tem_GZMK
E04_Vein_ACKR1
I05_CD16loNK_SELL
M01_cDC1_CLEC9A
M02_cDC2_CD1C
M03_cDC_LAMP3
S04_Fb_CD9
B04_Bm_CD27
B05_Bm_NR4A2
B06_Bm_ITGB1
CD4T01_Tn_SOX4
CD4T02_Tn_CCR7
CD4T08_Treg_FOXP3
CD8T01_Tn_CCR7
CD8T02_Tem_GZMK
M04_pDC_ULBP4
S02_Fb_C7
E01_Artery_IGFBP3
E02_Capillary_CA4
S13_Pericyte_CD36
S14_SMC_RERGL
S17_CMC_TNNT2
CD4T07_Tem_GZMK
CD8T05_Temra_GZMH
E03_Capillary_VIPR1
I04_CD16hiNK_HSPA1A
M07_Mph_FCN1
M11_Mph_PPARG
CD4T06_Tm_ANXA1
CD8T03_Tm_ITGA1
E04_Vein_ACKR1
M08_Mph_NLRP3
S06_Fb_ARID5B
S09_Fb_CEBPB
S10_Fb_MXRA5
Tissue
Bladder
Blood
Bone Marrow
Breast
Colon
Common Bile Duct
Esophagus
Eye
Fat
Heart
Kidney
Liver
Lung
Lymph Node
Nose
Omentum
Oral mucosa
Ovary
Pancreas
Prostate
Rectum
Salivary Gland
Skeletal Muscle
Skin
Small Intestine
Spleen
Stomach
Testis
Thymus
Tongue
Trachea
Ureter
Uterus
Vagina
Vasculature

Supplementary Fig. 5 | CM activities.

Scatter plots showing the correlation between CM activities and the frequencies of cell-subset components. Dots represent individual samples colored by tissues.

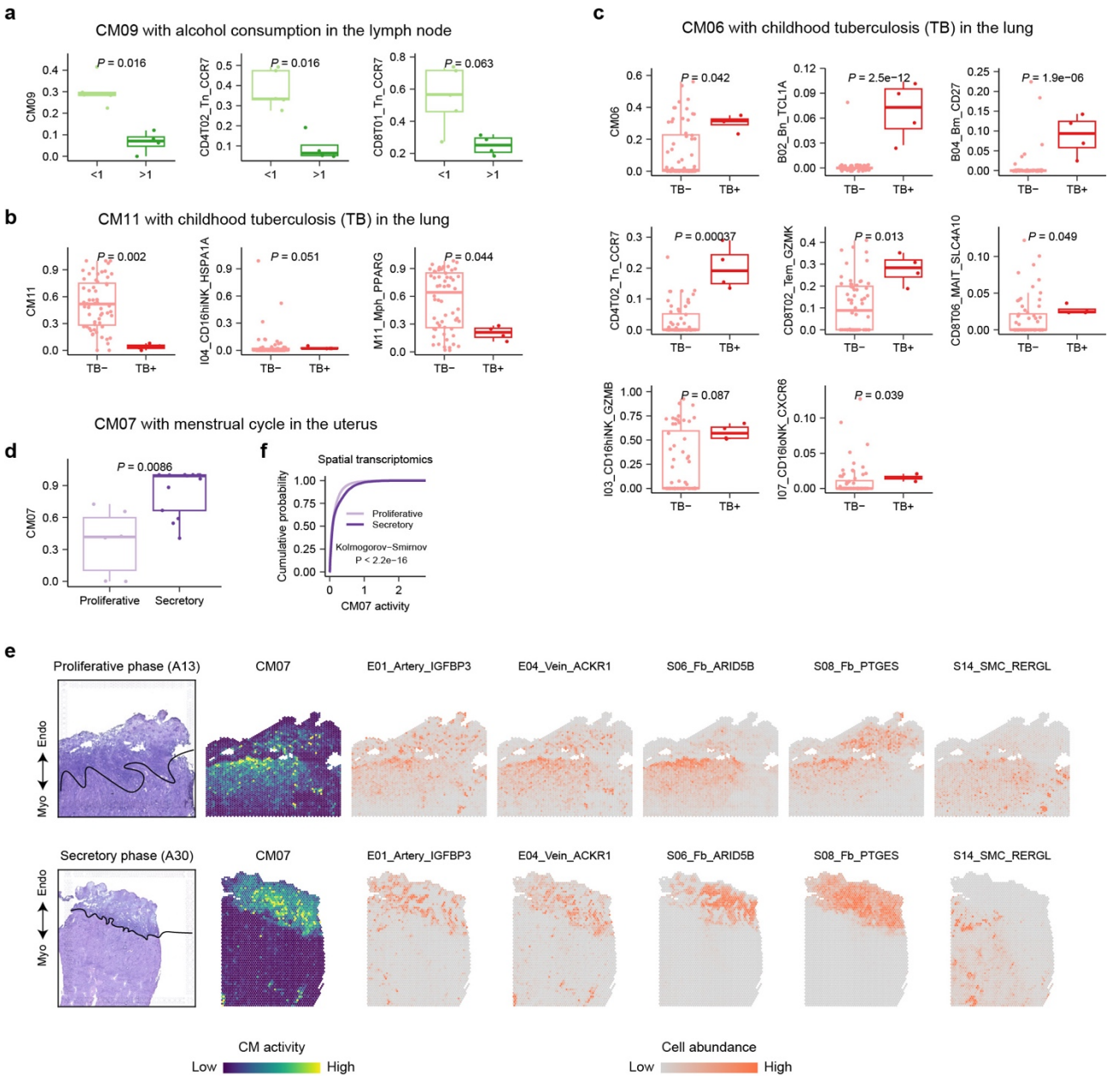

Supplementary Fig. 6 | Associations between CM activity and phenotypic factors.

(**a**) CM09 activity and frequencies of its subsets in individual lymph node samples stratified by alcohol consumption. Two-tailed unpaired Wilcoxon tests. (**b-c**) CM11 activity (**b**) and CM06 activity (**c**) alongside frequencies of their subsets in individual lung samples stratified by history of childhood tuberculosis. Two-tailed unpaired Wilcoxon tests. (**d**) CM07 activity in individual uterus samples stratified by menstrual phases. Two-tailed unpaired Wilcoxon tests. (**e**) Spatial distribution of CM07 and its cell subsets in two Visium sections of proliferative (top) and secretory (bottom) uterus. (**f**) Cumulative probability curves of CM07 activity in proliferative and secretory uterus. For box plots in **a-d**, the center line represents the median, the box limits represent the upper and lower quartiles, and the whiskers extend to the highest and lowest values within 1.5× the interquartile range.

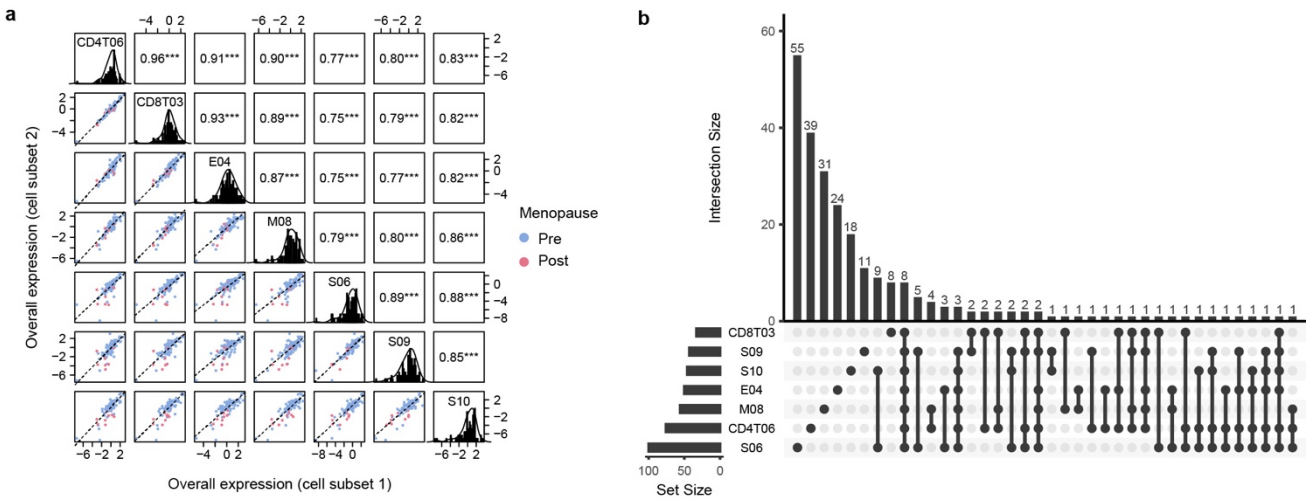

Supplementary Fig. 7 | DIALOGUE analysis of CM12.

(**a**) Diagonal panels: Distribution of MCP overall expression and kernel density estimates for individual cell-subset components. Down triangular panels: pairwise comparisons of overall expression scores for each cell component across samples. Dots represent individual samples (blue: pre-menopausal, red: post-menopausal). The dotted lines represent the linear fit. Upper triangular panels: pairwise Pearson correlation coefficients and significance (***$P < 0.001$, one-tailed mixed-effects test). (**b**) UpSet plot showing the overlap of MCP genes of CM12 cell subsets.

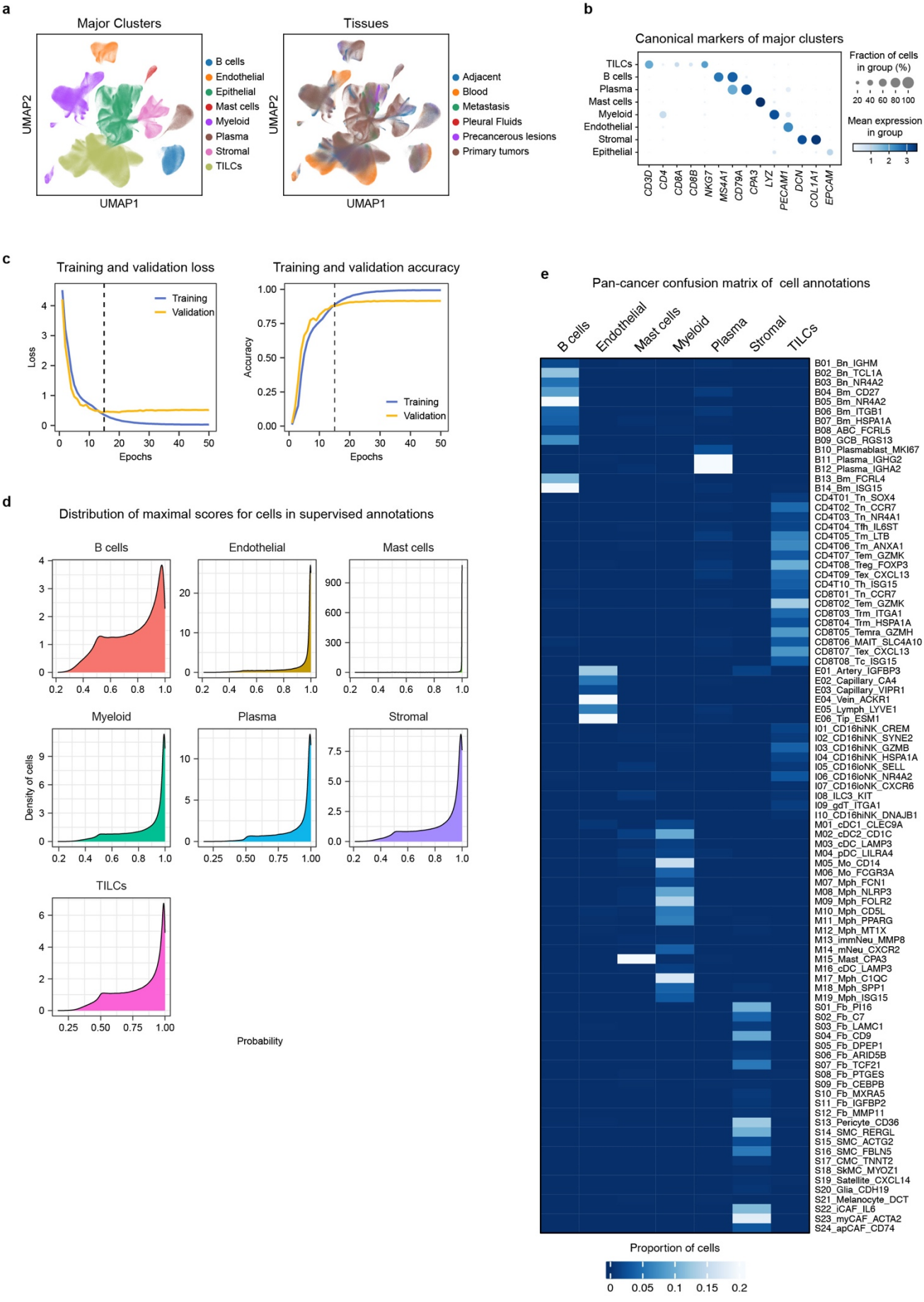
a
Major Clusters
UMAP2
UMAP1
B cells
Endothelial
Epithelial
Mast cells
Myeloid
Plasma
Stromal
TILCs
Tissues
Adjacent
Blood
Metastasis
Pleural Fluids
Precancerous lesions
Primary tumors
b
Canonical markers of major clusters
TILCs
B cells
Plasma
Mast cells
Myeloid
Endothelial
Stromal
Epithelial
CD3D
CD4
CD8A
CD8B
NKG7
MS4A1
CD79A
CPA3
LYZ
PECAM1
DCN
COL1A1
EPCAM
Fraction of cells in group (%)
20 40 60 80 100
Mean expression in group
1 2 3
c
Training and validation loss
Loss
Epochs
Training
Validation
Training and validation accuracy
Accuracy
d
Distribution of maximal scores for cells in supervised annotations
B cells
Endothelial
Mast cells
Myeloid
Plasma
Stromal
TILCs
Density of cells
Probability
e
Pan-cancer confusion matrix of cell annotations
B cells
Endothelial
Mast cells
Myeloid
Plasma
Stromal
TILCs
B01_Bn_IGHM
B02_Bn_TCL1A
B03_Bn_NR4A2
B04_Bm_CD27
B05_Bm_NR4A2
B06_Bm_ITGB1
B07_Bm_HSPA1A
B08_ABC_FCRL5
B09_GCB_RGS13
B10_Plasmablast_MKI67
B11_Plasma_IGHG2
B12_Plasma_IGHA2
B13_Bm_FCRL4
B14_Bm_ISG15
CD4T01_Tn_SOX4
CD4T02_Tn_CCR7
CD4T03_Tn_NR4A1
CD4T04_Tfh_IL6ST
CD4T05_Tm_LTB
CD4T06_Tm_ANXA1
CD4T07_Tem_GZMK
CD4T08_Treg_FOXP3
CD4T09_Tex_CXCL13
CD4T10_Th_ISG15
CD8T01_Tn_CCR7
CD8T02_Tem_GZMK
CD8T03_Trm_ITGA1
CD8T04_Trm_HSPA1A
CD8T05_Temra_GZMH
CD8T06_MAIT_SLC4A10
CD8T07_Tex_CXCL13
CD8T08_Tc_ISG15
E01_Artery_IGFBP3
E02_Capillary_CA4
E03_Capillary_VIPR1
E04_Vein_ACKR1
E05_Lymph_LYVE1
E06_Tip_ESM1
I01_CD16hiNK_CREM
I02_CD16hiNK_SYNE2
I03_CD16hiNK_GZMB
I04_CD16hiNK_HSPA1A
I05_CD16loNK_SELL
I06_CD16loNK_NR4A2
I07_CD16loNK_CXCR6
I08_ILC3_KIT
I09_gdT_ITGA1
I10_CD16hiNK_DNAJB1
M01_cDC1_CLEC9A
M02_cDC2_CD1C
M03_cDC_LAMP3
M04_pDC_LILRA4
M05_Mo_CD14
M06_Mo_FCGR3A
M07_Mph_FCN1
M08_Mph_NLRP3
M09_Mph_FOLR2
M10_Mph_CD5L
M11_Mph_PPARG
M12_Mph_MT1X
M13_immNeu_MMP8
M14_mNeu_CXCR2
M15_Mast_CPA3
M16_cDC_LAMP3
M17_Mph_C1QC
M18_Mph_SPP1
M19_Mph_ISG15
S01_Fb_PI16
S02_Fb_C7
S03_Fb_LAMC1
S04_Fb_CD9
S05_Fb_DPEP1
S06_Fb_ARID5B
S07_Fb_TCF21
S08_Fb_PTGES
S09_Fb_CEBPB
S10_Fb_MXRA5
S11_Fb_IGFBP2
S12_Fb_MMP11
S13_Pericyte_CD36
S14_SMC_RERGL
S15_SMC_ACTG2
S16_SMC_FBLN5
S17_CMC_TNNT2
S18_SkMC_MYOZ1
S19_Satellite_CXCL14
S20_Glia_CDH19
S21_Melanocyte_DCT
S22_iCAF_IL6
S23_myCAF_ACTA2
S24_apCAF_CD74
Proportion of cells
0 0.05 0.1 0.15 0.2

Supplementary Fig. 8 | Pan-cancer cell annotations.

(**a**) UMAP visualization of total cells colored by major clusters (left) or tissues (right). (**b**) Dot plot showing the expression of canonical markers for major clusters. (**c**) Selection of the epoch number for supervised cell annotations. (**d**) Distribution of maximal scores for cells in supervised annotations across individual major clusters. (**e**) Pan-cancer confusion matrix of non-epithelial cell annotations.

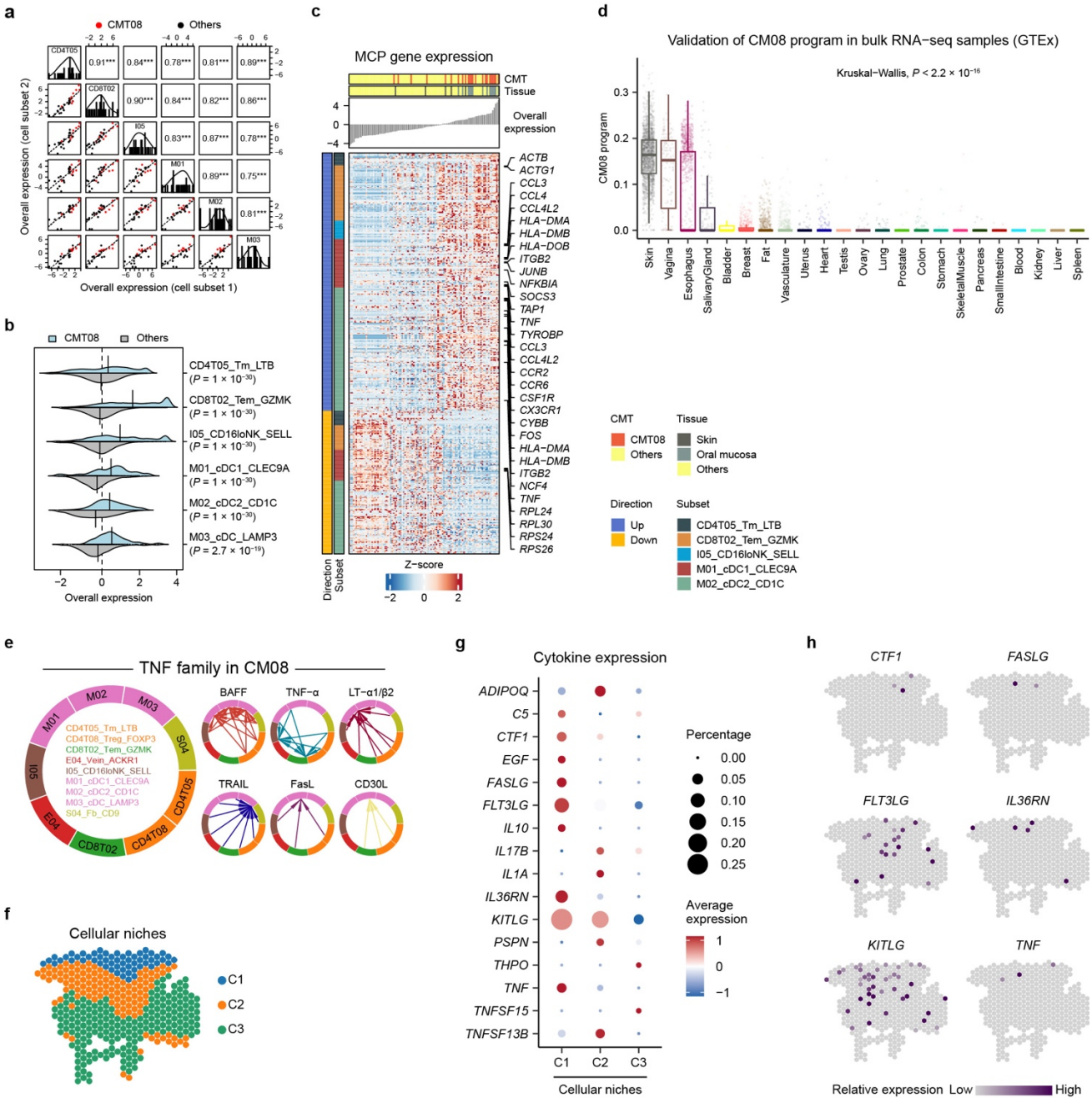

Supplementary Fig. 9 | CM08 program and cytokine analysis.

(**a**) Diagonal panels: distribution of MCP overall expression and kernel density estimates for individual cell-subset components. Down triangular panels: pairwise comparisons of MCP overall expression across samples. Dots represent individual samples colored according to CMT phenotypes. The dotted lines represent the linear fit. Upper triangular panels: pairwise Pearson correlation coefficients and significance (***$P < 0.001$, one-tailed mixed-effects test). (**b**) Distribution of MCP overall expression across different cell subsets for cells from CM08 or other CMTs. Vertical black line indicates the mean of the distribution. One-tailed mixed-effects model P values are shown. (**c**) Sample-averaged expression of MCP genes (rows) across samples (columns). Genes are sorted by their direction and pertaining cell subsets (left color bars), while samples are sorted by overall expression (top bar plot).

Samples are labeled by CMT phenotypes and tissue types (top color bar). (**d**) Box plots showing CM08 program expression across tissues. Dots represent individual samples profiled by bulk RNA-seq in GTEx. Tissues are ordered by the mean of CM08 program expression across samples. (**e**) TNF-family cytokine networks of CM08. (**f**) Spatial cellular niches identified by CellCharter in a Visium section of the skin. (**g**) Cytokine gene expression profiles across the cellular niches in **f**. Only cytokines detected by spatial transcriptomics data are shown. (**h**) Spatial distribution of selected cytokines in the Visium section in **f**. For the box plots in **d**, the center line represents the median, the box limits represent the upper and lower quartiles, and the whiskers extend to the highest and lowest values within 1.5× the interquartile range.

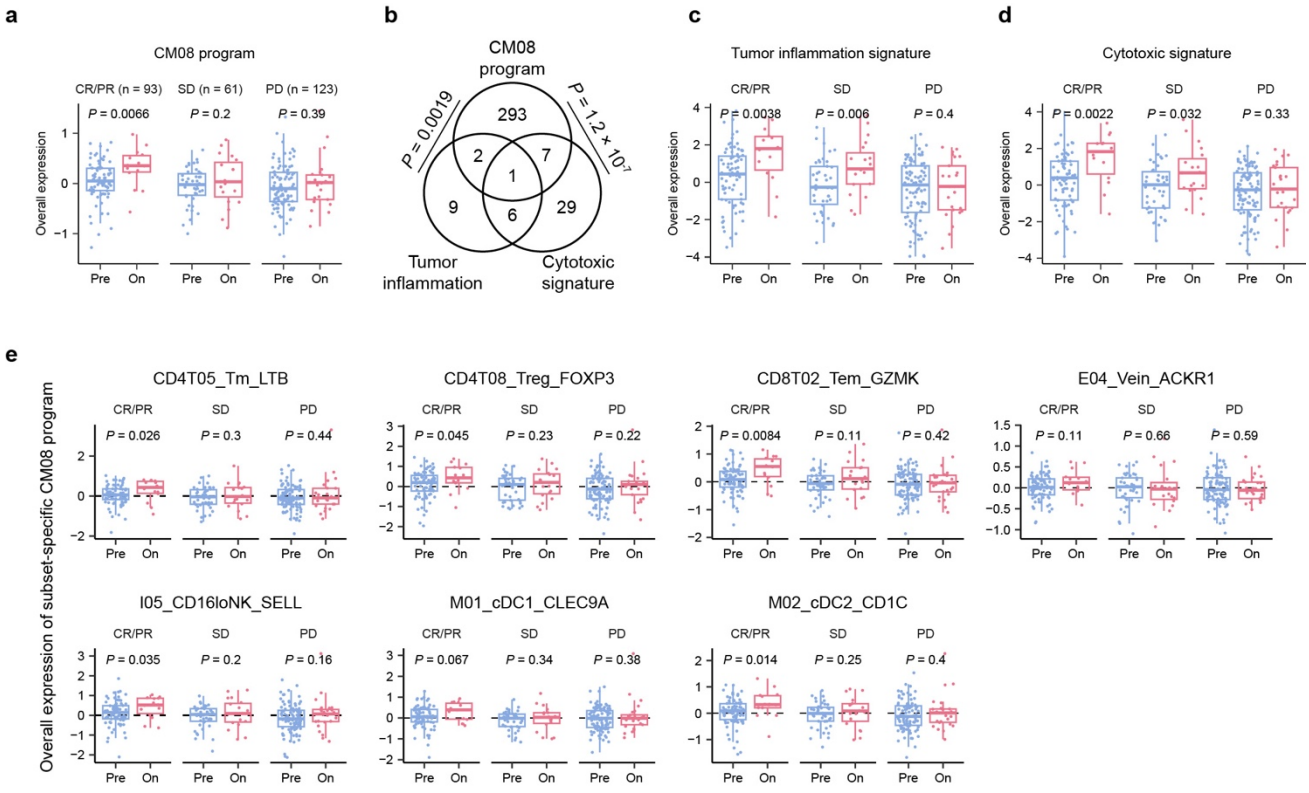

Supplementary Fig. 10 | Clinical implications of CM08 program.

(**a,c,d**) Overall expression of the CM08 program (a), tumor inflammation signature (c), and cytotoxic signature (d) in 277 bulk RNA-seq from 226 patients with advanced melanoma before (pre) and on PD-1 blockade therapies, stratified to responders (CR/PR) and non-responders (SD and PD). One-tailed unpaired Wilcoxon tests. (**b**) Venn diagram illustrating the overlap of signature genes of the CM08 program, tumor inflammation signature, and cytotoxic signature. The *P* values are calculated with hypergeometric tests. (**e**) The same plot as in **a** but showing the gene expression of individual cell subsets. Two-tailed paired Wilcoxon tests. For the box plots in **a** and **c-e**, the center line represents the median, the box limits represent the upper and lower quartiles, and the whiskers extend to the highest and lowest values within 1.5× the interquartile range. CR, complete response; PR, partial response; SD, stable disease; PD, progression disease.

Supplementary Notes

Supplementary Note 1 | **Linking CM activity to phenotypes**

To further investigate the significance of CMs, we assessed CM associations with phenotypic data. We observed a correlation between alcohol consumption and increased CM09 activity in lymph nodes (Supplementary Fig. 6a). Additionally, adult lung tissues with a history of childhood tuberculosis displayed increased immune CM06 activity compared to those without such a history (Supplementary Fig. 6b-c), reminiscent of the persistence of immune scars within the lung tissues following infection. Interestingly, the uterus-enriched CM07 exhibited higher activity in the endometrium during the secretory phase compared to the proliferative phase (Supplementary Fig. 6d-f), potentially indicating vascular remodeling associated with the menstrual cycle. Together, these results demonstrate that CMs provide a scaffold for multicellular investigation into the phenotypic associations with cellular diversity. Further research with larger cohorts is needed to comprehensively unveil CM associations with broader phenotypes.

Supplementary Note 2 | **A healthy multicellular program linked to cancer immunotherapy**

We focused our investigation on CM08, whose components exhibited moderate spatial consistency (Fig. 3f) but engaged the most cytokines among CMs (Extended Data Fig. 6g). As previously noted, CM08 was enriched in barrier tissues such as the skin, oral mucosa, and other exposed areas (Fig. 2c-d), where the mucosa plays a key role as the first line of defense against pathogens.

The DIALOGUE analysis identified an MCP, which we termed the "CM08 program" for its substantial upregulation in CMT08 (primarily skin and oral mucosa) compared to non-CMT08 samples ($P < 2.7 \times 10^{-19}$, mixed-effects test) (Supplementary Fig. 9a-c). This program was associated with inflammatory responses, such as the Toll-like receptor signaling pathway (*CCL3*, *CCL4*, and *FOS*), antigen processing (*HLA-DMA*, *HLA-DMB*, *HLA-DOB*, and *TAP1*), and the TNF signaling pathway (*TNF*, *JUNB*, *NFKBIA*, and *SOCS3*) (FDR < 0.01, hypergeometric test) (Supplementary Table 10). Using GTEx RNA-seq data, we validated that the CM08 program was most abundant in the skin (Supplementary Fig. 9d), consistent with the intrinsic characteristics of barrier tissues constantly exposed to the external environment. Cytokine analysis and spatial validation indicated that the CM08-associated niche may be primarily driven by the TNF family members (Extended Data Fig. 5a-b and Supplementary Fig. 9e-h). These findings suggest that CM08 represents an interplay between innate and adaptive immunity, supported by recent reports showing that acute skin infection can induce tissue-resident memory-like natural killer (NK) cells[1].

Further, we hypothesized that the CM08 program from healthy context may have clinical implications, particularly for cancer immunotherapy. To explore this, we examined the association of the CM08 program with patient responses to immunotherapy. Using an RNA-seq cohort of 226 patients with advanced melanoma treated with PD-1 blockade therapies[2], we found that the CM08 program showed

higher expression in on-treatment samples from responders compared to pre-treatment samples (Supplementary Fig. 10a). Such changes were not observed in non-responders (Supplementary Fig. 10a), suggesting that the CM08 program could serve as an indicator of treatment efficacy.

To further assess the relevance of the CM08 program in the context of known immunotherapy markers, we compared it to established indicators such as tumor inflammation[3] and cytotoxic signature[4]. Only a few genes were shared between the CM08 program and these signatures (Supplementary Fig. 10b), underscoring that the CM08 program is specific to the intrinsic features of barrier tissues under healthy condition, rather than being directly tied to the tumor microenvironment. This reinforces the importance of the CM08 program in understanding immune properties in both healthy and disease contexts. Additionally, we compared their performance in predicting treatment efficacy in melanoma patients undergoing anti-PD-1 therapy. Tumor inflammation and cytotoxic signatures showed increased expression upon treatment in patients with a complete (CR) or partial (PR) response, as well as with those with stable disease (SD). In contrast, such change in CM08 program was only observed in responders (CR and PR) and absent in non-responders (SD) (Supplementary Fig. 10c-d). Notably, this coordinated multicellular response was also evident within individual cell subsets of CM08 (Supplementary Fig. 10e), reinforcing the concept of functional coordination among these cell subsets within the CM08. These findings suggest that the CM08 program may be a more precise indicator of treatment efficacy for anti-PD-1 therapy. Further investigation is needed to fully uncover the mechanisms linking multicellular properties in homeostasis with pathological conditions.

Supplementary Table legends

Supplementary Table 1. Overview of pan-tissue single-cell datasets
Supplementary Table 2. Differently expressed genes of fibroblast subsets
Supplementary Table 3. Overview of spatially resolved transcriptomics datasets
Supplementary Table 4. Responsive cytokines in healthy CMs
Supplementary Table 5. CM05 regulons inferred by pySCENIC
Supplementary Table 6. Gene list of CM12 MCP in the breast
Supplementary Table 7. Overview of pan-cancer single-cell datasets
Supplementary Table 8. Cancer type abbreviations and full names
Supplementary Table 9. Cancer-associated cell subsets
Supplementary Table 10. Gene list of CM08 MCP
Supplementary Table 11. Responsive cytokines in cCM02
Supplementary Table 12. Gene list of cCM02 MCP

Supplementary References

1 Torcellan, T. *et al.* Circulating NK cells establish tissue residency upon acute infection of skin and mediate accelerated effector responses to secondary infection. *Immunity* **57**, 124–140.e127 (2024).

2 Campbell, K. M. *et al.* Prior anti-CTLA-4 therapy impacts molecular characteristics associated with anti-PD-1 response in advanced melanoma. *Cancer Cell* **41**, 791–806 e794 (2023).

3 Ayers, M. *et al.* IFN-γ-related mRNA profile predicts clinical response to PD-1 blockade. *J. Clin. Invest.* **127**, 2930–2940 (2017).

4 Bagaev, A. *et al.* Conserved pan-cancer microenvironment subtypes predict response to immunotherapy. *Cancer Cell* **39**, 845–865 e847 (2021).